FISEVIER

Contents lists available at ScienceDirect

Optics Communications

journal homepage: www.elsevier.com/locate/optcom



A new method for detecting the nonlinearity of the Pancharatnam phase of light



Hyrum Richardson a,b, Charlotte Welch a,c, Sean Nomoto a, Reeta Vyas a, Surendra Singh a,*

- ^a Department of Physics, University of Arkansas, Favetteville, AR 72701, USA
- b Institute of Optics, University of Rochester, Rochester, NY 14627, USA
- ^c Department of Physics, Florida State University, Tallahassee, FL 32306, USA

ARTICLE INFO

Keywords: Geometric phase Berry phase Pancharatnam phase of light Polarization Structured light beams

ABSTRACT

A method based on the tracking of the peaks of interference fringes as a function of time-dependent analyzer setting is used to detect the Pancharatnam phase of light. The advantage of this method is demonstrated by observations of the nonlinearity of the Pancharatnam phase for certain paths on Poincare sphere where the fringe visibility reduces to almost zero. We also describe variations of this experiment with structured light beams, where the Pancharatnam phase leads to linear or nonlinear rotation of flower-pattern or spiral-shape interference fringes.

1. Introduction

Polarization is a physical degree of freedom of an electromagnetic wave. If the polarization state of a light wave evolves during its propagation, the wave may acquire a contribution to its phase in addition to the contribution from its dynamical phase. This additional, polarization-dependent contribution to the phase of a light wave, was first discussed by Pancharatnam [1] and is known as the Pancharatnam phase of light. It is a type of geometric phase of light [2]. Pancharatnam showed that for cyclic evolution of polarization, this phase depends only on the geometry of the geodesic circuit traced by the wave polarization on the Poincare sphere and is equal to half the area enclosed by the polarization circuit on the Poincare sphere [3]. Experimental observations of the Pancharatnam phase of light typically involve an interferometric set up where the polarization of one or both of the two interfering coherent beams evolves as they traverse the interferometer. At the output of the interferometer, the beams interfere with a phase that includes contribution from the dynamical phase difference which arises due to the difference in the paths traversed by the beams as well as the Pancharatnam phase.

The dependence of the Pancharatnam phase on the orientation, retardation, and other parameters pertaining to polarization elements affecting wave polarization is, in general quite complex; it may be nonlinear [4–6] or linear [7–9], depending on the polarization paths on the Poincare sphere. While both linear and linear regimes of the Pancharatnam phase are of interest from a fundamental point of view, the nonlinear regime is of special interest from an application point of view. Indeed, the nonlinear aspect of the Pancharatnam phase has been used for optical switching [6,10] as well as supersensitive polarization

interferometry [11]. The concept of the Pancharatnam phase has been extended to quantum optical and atom optical systems as well [12–14].

The experiments to observe the Pancharatnam phase have been summarized in several review articles [15,16]. Most experiments have used polarization circuits which lead to linear dependence of the Pancharatnam phase on the parameter that affects the change. These experiments, typically observe the Pancharatnam phase by changing the orientation of polarizers in small increments and/or retarders and monitoring the fringe intensity. This approach works well in the linear regime but is not convenient in the nonlinear regime. The main difficulty arises from the fact that the fringe intensity variation at a fixed point arises both from the change in the phase difference and the intensities of the two interfering beams but is, in fact, dominated by the variation in beam intensities [6]. We propose and demonstrate that by making the polarization settings time-dependent and monitoring the positions of interference fringe peaks is a more efficient way to observe the Pancharatnam phase. The advantage of the method described in this paper is especially transparent in the context of the nonlinearity of the Pancharatnam phase.

We begin by first focusing on how the nonlinearity of the Pancharatnam's phase arises. This is followed by an experimental observation of the nonlinearity using the method proposed here when a fundamental Gaussian beam is used in the interferometer. We also describe experiments using structured beams for observing the Pancharatnam phase both in the linear and nonlinear regimes and their distinguishing features.

E-mail address: ssingh@uark.edu (S. Singh).

Corresponding author.

2. Nonlinear Pancharatnam phase

Consider the Mach-Zehnder interferometer shown in Fig. 1(a) and the corresponding Poincare sphere [17] in Fig. 1(b) showing the trajectory of the polarization corresponding to the beams in the two arms of the interferometer. A vertically polarized (point V on the Poincare sphere) light beam of wavelength λ is incident at a 50/50 beam splitter BS₁. The beam along arm A of the interferometer passes through a half-wave plate H₁ with its fast axes oriented at 45° to the horizontal, while the beam along arm B passes a half-wave plate H2 (designed for a slightly longer wavelength $\lambda + \Delta \lambda$) with its fast axis at 45° to the horizontal. The beam traversing arm A arrives horizontally polarized (point H on the Poincare sphere) at beam splitter BS₂ while the beam traversing arm B arrives elliptically polarized (point B) with its long axis horizontal. The beams emerging from one of the output ports of BS2 are incident on a linear polarizer LP (analyzer) with its transmission axis at an angle φ to the horizontal. The analyzer projects the polarization states of the two beams onto the polarization state C (linear polarization at an angle φ to the horizontal). Note that the angle of azimuth of state C on Poincare sphere is twice the angle φ specifying the inclination of the analyzer axis to the horizontal [17]. Thus the beams emerging from the analyzer LP are linearly polarized in state C and interfere with a phase difference, which equals the sum of the dynamical phase due to optical path length difference between the two arms of the interferometer and the Pancharatnam phase given by half the area enclosed by the spherical triangle HBC on the Poincare sphere [Fig. 1(b)].

The Pancharatnam phase contribution to the phase difference between the two wave interfering at the output of analyzer LP is half the area of spherical triangle HBC, which can be expressed in terms of the coordinates of points H, B and C on Poincare sphere [5]. It can also be expressed directly in terms of experimentally accessible quantities using Jones matrix formalism [17]. To do so, we recall that the Jones matrix $M_\xi(\varphi)$ of a wave plate whose fast axis is inclined at an angle φ to the horizontal and which introduces a phase difference δ between its slow and fast eigenstates is

$$M_{\xi}(\varphi) = \begin{pmatrix} \cos^2 \varphi + \xi \sin^2 \varphi & (1 - \xi) \sin \varphi \cos \varphi \\ (1 - \xi) \sin \varphi \cos \varphi & \xi \cos^2 \varphi + \sin^2 \varphi \end{pmatrix}, \tag{1}$$

where $\xi=\exp[i\delta]$ for a wave plate and by putting $\xi=0$ we obtain Jones matrix $L_o(\varphi)$ for a linear polarizer.

The initial state of light of wavelength λ_1 entering the interferometer is vertical polarization (V on the Poincare sphere) represented by Jones matrix $\begin{pmatrix} 0 \\ 1 \end{pmatrix}$. Noting that the half-wave plate (designed for λ_1) in arm A is inclined at $\varphi_A = \pi/4$ and introduces a retardation $\delta_A = \pi$ corresponding to $\xi_A = \exp[i\delta_A] = -1$, whereas the half-wave plate in arm B (designed for λ_2) is inclined at $\varphi_B = \pi/4$ and introduces a retardation $\delta_B = \pi(\lambda_2/\lambda_1) = \pi + \pi(\lambda_2 - \lambda_1)/\lambda_1$ corresponding to $\xi_B = \exp[i\delta_B] = -\exp[i\alpha]$, with $\alpha = \pi(\lambda_2 - \lambda_1)/\lambda_1$. Using Jones matrices for the retarders and polarizers for these values of φ and ξ , the final states of polarization of the two beams following the arms A and B of the interferometer, after the analyzer LP, are given by

$$\langle A| = L_{\sigma}(\varphi) M_{\xi_{A}}(\pi/4) \begin{pmatrix} 0 \\ 1 \end{pmatrix}$$

$$= \begin{pmatrix} \cos^{2} \varphi & \sin \varphi \cos \varphi \\ \sin \varphi \cos \varphi & \sin^{2} \varphi \end{pmatrix} \begin{pmatrix} 0 & 1 \\ 1 & 0 \end{pmatrix} \begin{pmatrix} 0 \\ 1 \end{pmatrix} ,$$

$$= \cos \varphi \begin{pmatrix} \cos \varphi \\ \sin \varphi \end{pmatrix} ,$$

$$(2)$$

$$\begin{split} \langle B| &= L_o(\varphi) M_{\xi_B}(\pi/4) \begin{pmatrix} 0 \\ 1 \end{pmatrix} \\ &= \begin{pmatrix} \cos^2 \varphi & \sin \varphi \cos \varphi \\ \sin \varphi \cos \varphi & \sin^2 \varphi \end{pmatrix} \frac{1}{2} \begin{pmatrix} (1+\xi_B) & (1-\xi_B) \\ (1-\xi_B) & (1+\xi_B) \end{pmatrix} \begin{pmatrix} 0 \\ 1 \end{pmatrix} \,, \end{split}$$

$$= \frac{1}{2} \left[\cos \varphi (1 - \xi_B) + \sin \varphi (1 + \xi_B) \right] \begin{pmatrix} \cos \varphi \\ \sin \varphi \end{pmatrix}. \tag{3}$$

The preceding calculation takes into account only the phase due to the evolution of wave polarization. From Eqs. (2) and (3), the phase difference (which equals the Pancharatnam phase within a constant), between the two interfering beams after the analyzer, arising from the evolution of polarization, is given by

$$\gamma_{P} = \tan^{-1} \left[\frac{\sin \alpha (\cos \varphi - \sin \varphi)}{(\cos \varphi + \sin \varphi) + \cos \alpha (\cos \varphi - \sin \varphi)} \right]. \tag{4}$$

This is clearly a highly nonlinear function of the analyzer angle φ . The rate of change $\gamma_p' \equiv d\gamma_p/d\varphi$ of the Pancharatnam phase with the analyzer angle φ is given by

$$\gamma_p' = -\frac{\sin \alpha}{1 + \cos \alpha \cos 2\omega} \,, \tag{5}$$

which depends on angle α by which the point B overshoots linear polarization H on the Poincare sphere. For small analyzer angles ($\varphi \approx 0$), the magnitude of γ'_p is $\tan(\alpha/2)$ whereas for analyzer angles near $\pi/2$ it is $\cot(\alpha/2)$. This means that for small values of α , the Pancharatnam phase varies little ($\gamma'_p \sim \alpha/2$) with analyzer settings φ near zero, whereas it varies rapidly ($\gamma'_p \sim 2/\alpha$) for analyzer settings close to $\pi/2$. The smaller the angle α , the more pronounced the nonlinearity of the Pancharatnam phase for analyzer angles $\varphi \approx \pi/2$.

If the analyzer is rotated, the angle φ increases (or decreases), the final state C moves away from H towards V along the equator. As φ crosses $\pi/2$, the geodesic connecting B to C swings suddenly from the left half of the lower hemisphere to right half of the lower hemisphere passing over the south pole of Poincare sphere. The area of the spherical triangle HBC and, therefore, the Pancharatnam phase, follows this same trend, changing most rapidly as φ crosses the $\pi/2$ setting. In this case the Pancharatnam phase depends nonlinearly on the analyzer setting φ . Experimental verifications of the nonlinearity of the Pancharatnam phase have used similar interferometric setups that project polarization states of the two beams on to the same final polarization state using a variable analyzer [4–6].

The difficulty of such setups for observing the Pancharatnam phase can be appreciated by considering the resultant intensity I_c after the analyzer LP (transmitting polarization C), which is given by [1]

$$\begin{split} I_C &= I_H \cos^2\left(\frac{1}{2}\theta_{HC}\right) + I_B \cos^2\left(\frac{1}{2}\theta_{BC}\right) \\ &+ 2\sqrt{I_H I_B} \cos\left(\frac{1}{2}\theta_{HC}\right) \cos\left(\frac{1}{2}\theta_{BC}\right) \cos(\delta + \gamma_P), \end{split} \tag{6}$$

where $I_{_H}$ and $I_{_B}$ are the intensities of the beams with polarizations H and B, respectively, $\theta_{_{HC}}$ and $\theta_{_{BC}}$ are the angles between the polarization states H and C, and B and C, respectively, on the Poincare sphere, δ is the dynamical phase difference (depends on the location of the fringe) and $\gamma_{_{P}}$ is the Pancharatnam phase. As point C moves all three quantities, θ_{HC} , θ_{BC} , and γ_P [Eq. (4)] vary and this means that the resultant intensity I_C will vary both due to the changes in the intensities of the two beams and the change in the Pancharatnam phase and for the polarization circuit shown, the intensity variation of the interfering beams dominates the resultant intensity variation masking the effect of phase nonlinearity. This makes the extraction of phase difference by monitoring the fringe intensity difficult [6]. The approach used in this paper to address this problem is to make the analyzer setting time dependent and focus on the motion of the position of the peaks rather than on the fringe intensity as the analyzer setting changes. Note that the position of an interference fringe peak of order m, given by $\delta_m + \gamma_p =$ $2\pi m \Rightarrow \delta_m = 2\pi m - \gamma_p$, is determined solely by the change in phase γ_p . Note that the measurement of the position of a fringe peak certainly involves a measurement of intensity, but it is not the measurement of the intensity at one point (the peak) but of the entire intensity pattern. As explained in Section 4, the peak positions are located by fitting a cosine curve to the entire pattern. This procedure makes the location of fringe peaks a global quantity rather than a local one, allowing the determination of the peak position with greater accuracy even if the

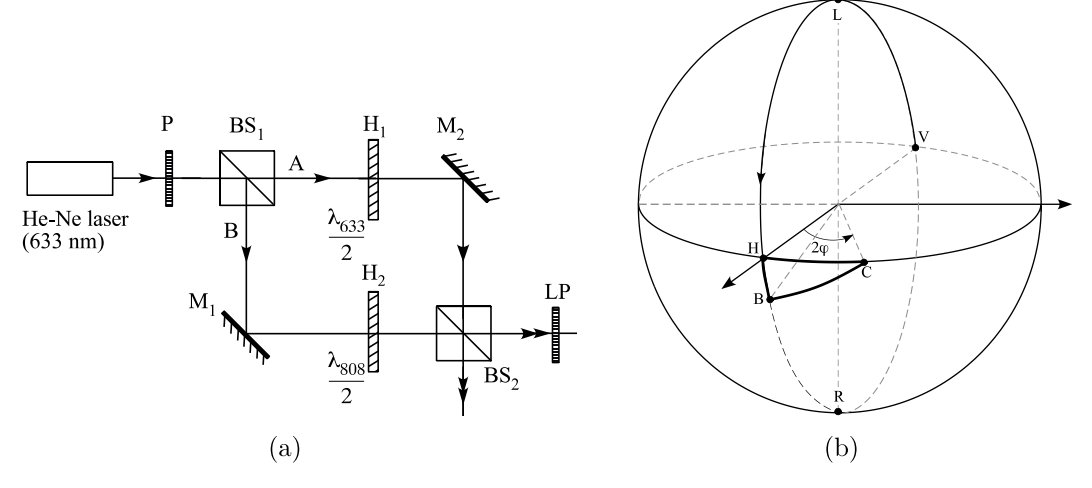


Fig. 1. (a) Mach–Zehnder interferometer for observing the nonlinearity of the Pancharatnam phase. (b) Polarization trajectories for the two interferometer beams on the Poincare sphere.

overall intensity decreases and becomes small. We find that even in cases where the amplitudes of the interfering beams do not change as the polarization evolves [see the next section], monitoring the peak position is at least as effective as monitoring the fringe intensity for observing the Pancharatnam phase of light.

3. Experiment

The experimental set up is shown in Fig. 1(a). A 50/50 beam splitter BS $_1$ divides a vertically polarized (V) laser beam ($\lambda_1=633$ nm) into two coherent waves of equal intensity and sends one part along arm A and the other along arm B. Half-wave plate H $_1$ with its fast axis at $\pi/4$ to the horizontal, transforms the polarization state of the wave along arm A into horizontal polarization H along great circle VLH on the Poincare sphere and the half-wave plate in arm B, designed for $\lambda_2=808$ nm, transforms the wave along this arm into elliptic polarization B along the great circle VLHB. The analyzer LP projects states H and B onto state C (linear polarization at an angle φ to the horizontal). The analyzer LP is mounted on a voltage controlled motor whose angular speed can be controlled by a varying the voltage. For a fixed voltage, the motor rotates at a uniform angular speed and the final state C advances along the equator at a constant angular speed.

If the motor rotates at a constant angular speed Ω , the change in analyzer angle (with the horizontal) is given by $\varphi=\Omega t$, where the origin of time is chosen to be the instant when the analyzer is horizontal. The Pancharatnam phase contribution to the overall interference phase is then given by Eq. (4) with $\varphi=\Omega t$. Since the path difference between the two arms of the interferometer remains unchanged as the analyzer rotates, only the time varying Pancharatnam phase contributes to the change in the overall interference phase difference. Due to this timevarying phase difference we observe a shifting fringe pattern. Due to the nonlinearity of Pancharatnam phase, the fringes shift nonuniformly even as the analyzer rotates at a constant angular speed. The motor was rotated at a rate of approximately 1/9 Hz corresponding to $\Omega=(2\pi/9)$ rad/s. The camera sampled the resulting interference pattern at an average rate of 7 Hz.

4. Results and discussion

The interference pattern at the output of analyzer LP was monitored by a CCD camera. A few sample interference frames, separated by equal time intervals are shown in Fig. 2. The rapid shift of the fringe pattern due the Pancharatnam phase occurs between Figs. 2(d) and 2(e) (see the video Visualization1 in Fig. 2).

Successive image frames of the interference pattern, recorded at regular intervals, were analyzed using a computer program, which

took pixel brightness (corresponding to intensity) measurements along points on a fixed line in each frame of the series. As an example, the vertical red line in Fig. 3(a) shows the pixels along which fringe intensity measurements were taken. The line is four pixels wide, and the average of intensity over the four horizontal pixels inside the line was associated with the vertical pixel coordinate. The interference fringe pattern was constructed by plotting the vertical pixel coordinate along the x-axis and the intensity I(x) of that pixel on along the y-axis (Fig. 3(b)). The fringe-pattern was fitted to a cosine function

$$I(x) = a + b\cos(kx - d),\tag{7}$$

where the parameters a, b, and d varied from frame to frame reflecting variation of incident light intensity, nonuniform transmission by different parts of the analyzer, etc. but the parameter k, which is related to the periodicity of the fringe-pattern was the same for all frames. The parameter k is the wavenumber for the interference pattern, which was determined by performing a nonlinear regression on a few sample frames in the series. All the frames were then fitted with the cosine form (7) using this value of k. This assumption was made because the path lengths, wavelength of interfering beams and alignment of the setup remain unchanged and, therefore, the period of the interference pattern remains unchanged.

The camera was allowed to saturate at the highest fringe intensity (the orange seen in Fig. 3(a)) in order to be able to record fringe patterns even when the fringes became too dim for analyzer settings close to $\pi/2$.

Fig. 3(a) shows a typical fringe-pattern recorded by the CCD. It also shows a line along which the pattern was scanned. The result of this scanning is shown in Fig. 3(b), which displays intensity I(x) (dots) as a function of pixel coordinate x along with the cosine wave regression (continuous curve). This allowed us to determine the position of fringe peaks. By following this procedure for successive frames and recording the coordinate of each fringe peak we were able to track the position of each fringe peak from one frame to another. Using the fact that the phase difference from one interference fringe to the next changes by 2π , each peak position was assigned a relative phase difference. Finally, since successive frames were recorded at regular time intervals $\Delta t \approx (1/7)$ s, the analyzer angle from one frame to the next differed by $\Omega \Delta t$. The result is a graph of peak coordinates vs. analyzer angle shown in Fig. 4. Note that we have not made an attempt to align the zero of analyzer angle to a particular position of fringe peak. However, the shift of the fringe peak is directly related to the variation of the Pancharatnam phase due to the setting of the uniformly rotating analyzer.

The positions of the peaks of several interference fringes were tracked. This allows for a more efficient use of the data and also works

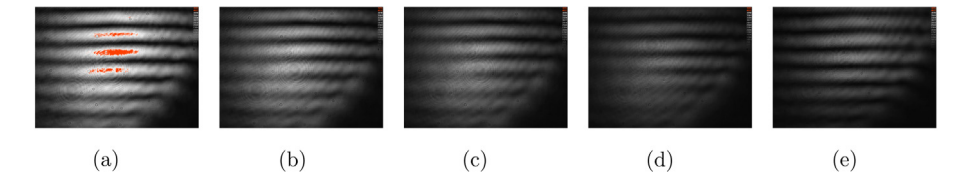


Fig. 2. Sample interference fringe pattern images recorded by the CCD camera. The fringes shift most rapidly as the analyzer angle crosses $\pi/2$ setting (see Visualization1).

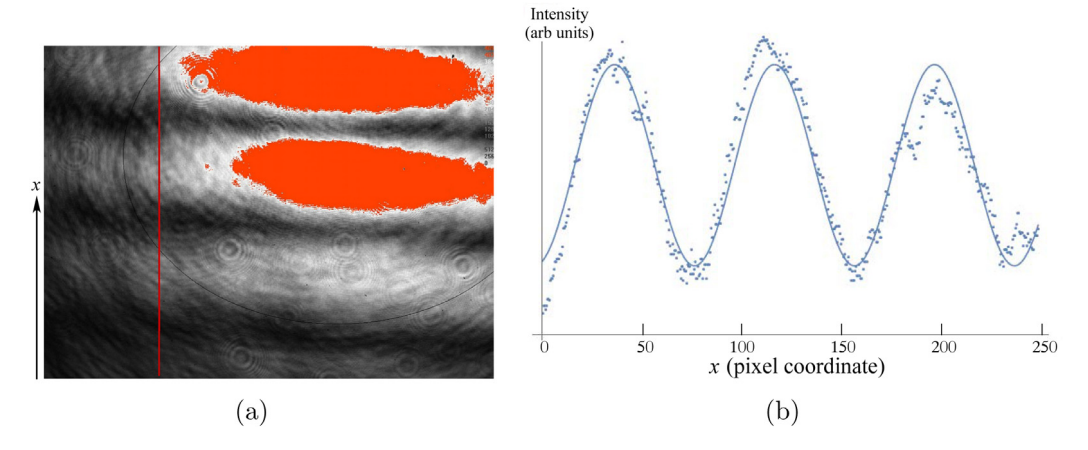


Fig. 3. (a) A typical frame of recorded interference fringes showing the line along which fringes were scanned. (b) Scanned fringe pattern (dots) along with the cosine wave regression (full curve).

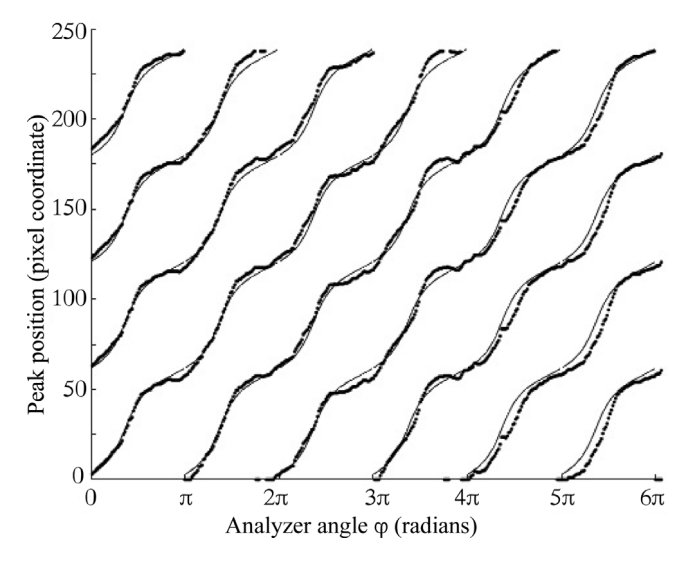


Fig. 4. Experimental data (black dots) for peak positions compared with the theoretical predictions (full curve) of Eq. (4).

as a check to detect any systematic drifts. The results are shown in Fig. 4. The vertical axis is the peak position (pixel coordinate), which as noted in the preceding paragraph, is proportional to the Pancharatnam Phase and the horizontal axis is the angle of rotation of the analyzer. The figure shows the trajectories of the peak positions of several fringes. The full curves are the predictions of Eq. (4).

We carried out another variation of this experiment using angular momentum carrying pure vortex beams [18]. A vortex beam of angular momentum index +2 was sent along one arm and another of opposite index -2 along the other arm of a well-aligned Mach–Zehnder interferometer in Fig. 1(a). A single four-lobe interference fringe pattern [Fig. 5] appears at the output of the analyzer [18]. As the Pancharatnam phase varies with the rotation of the analyzer, the

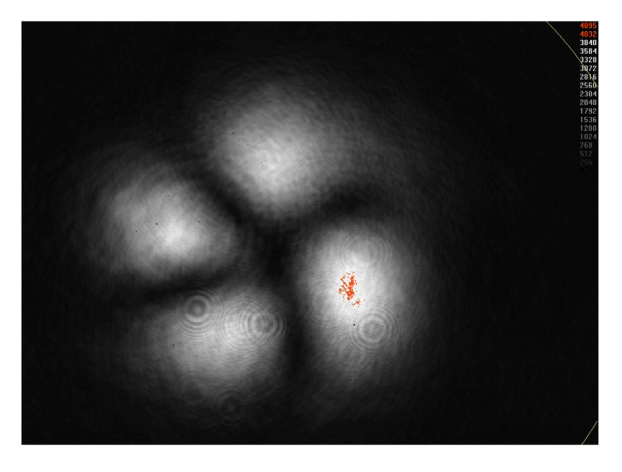


Fig. 5. Four-lobe fringe pattern when beams of opposite angular momentum index ± 2 traverse the two arms of the interferometer in Fig. 1(a). Nonlinear Pancharatnam phase causes rotation of the fringe pattern to speed up when the analyzer setting crosses $\varphi = \pi/2$ (see Visualization2).

relative phase difference between the two interfering beams also varies and causes a rotation of the interference pattern.

5. Conclusion

The experimental data from the interferometer agree with the predictions of Pancharatnam's theorem and, in particular, verify the nonlinear dependence of the Pancharatnam phase on analyzer angle. The scatter of points is due to the cumulative effect of small variations in intensity, rate of rotation, CCD sampling rate, and vibrations coupling into the optical setup. That many of the deviations of interferometer data from the theoretical curves are similar for all the fringes, suggests that they are caused by these common sources of error in the image acquisition system that affect the entire fringe pattern. We emphasize that by using the method proposed here, viz., by making the analyzer angle time-dependent and varying it at a constant rate, the motion of

the fringes at the output of the analyzer can be viewed on a screen (or on a computer screen connected to the CCD). Starting from a setting near $\varphi=0$, as the analyzer rotates and φ increases, the fringe pattern dims without much shift, but as φ crosses $\pi/2$ setting, the fringes shift rapidly and the fringe-pattern momentarily disappears. The effect is visually quite dramatic. The attached video [Fig. 2 Visualization1] of fringe pattern as a function of analyzer angle shows an example of this. It can be seen that as time elapses and analyzer angle changes linearly with time, fringes vary in intensity with little shift until the analyzer reaches $\pi/2$ setting, when the fringes momentarily vanish and the fringe pattern shifts.

The second video clip [Fig. 5 Visualization2] shows this when the two arms of the interferometer carry vortex beams of opposite indices ± 2 . In this case, as the analyzer rotates, fringes, which have the form of four flower petals, vary in intensity with little angular shift until the analyzer crosses $\pi/2$ setting when the fringe pattern rotates rapidly.

We have used the method proposed here for other interferometers [7–9] as well, where the Pancharatnam phase varies linearly with the angular setting of a wave plate, using both the fundamental Gaussian beam and higher order structured beams, such as the vortex beams. The use of vortex beams is attractive as the interference fringe pattern provides a reference point, the origin of a fork or a spiral in the fringe pattern, past which fringe movement can be monitored. In such cases one directly observes uniformly shifting or rotating spiral fringes past the reference point for a uniformly rotating analyzer, in agreement with the predictions of Pancharatnam's theorem.

Acknowledgments

Hyrum Richardson and Charlotte Welch were supported by the National Science Foundation Research Experiences for Undergraduate program, USA (NSF Award 1460754) and the University of Arkansas, USA. One of us (SS) would like to thank the Indian Institute of Technology, Madras for a visiting appointment, where a part of this work was completed.

Appendix A. Supplementary data

Supplementary material related to this article can be found online at https://doi.org/10.1016/j.optcom.2019.06.018.

References

- S. Pancharatnam, Generalized theory of interference, and its applications, Proc. Ind. Acad. Sci. A 44 (1956) 247–262, Also In Collected Works of S. Pancharatnam (Oxford U. Press, Oxford, 1975).
- [2] M.V. Berry, Quantal phase factors accompanying adiabatic changes, Proc. Roy. Soc. London 392 (1984) 45–57, and "The Adiabatic Phase and Pancharatnam's Phase for Polarized Light," J. Mod. Optics 34, 1401-1407 (1987). Both papers reprinted in Geometric Phases in Physics, A. Shapere and F. Wilczek, Ed. (World Scientific, Singapore, 1989). See also M.V. Berry, "Anticipations of the Geometric Phase," Physics Today, 41, 34-40 (1990).
- [3] P.K. Aravind, A simple proof of Pancharatnam's theorem, Opt. Commun. 94 (1992) 191–196.
- [4] H. Schmitzer, S. Klein, W. Dultz, Nonilinearity of Pancharatnam's topological Phase, Phys. Rev. Lett. 71 (1993) 1530–1533.
- [5] W. Dultz, S. Klein, Pancharatnam's phase in polarization optics, in: T.W. Barrett, D.M. Grimes (Eds.), Advanced Electromagnetism: Foundations, Theory and Applications, World Scientific, Singapore, 1995, pp. 357–375.
- [6] W. Li, L. Gong, Y. Gao, Y. Chen, Experimental observation of the nonlinearity of the Pancharatnam's phase with Michelson interferometer, Opt. Commun. 169 (1999) 17–22.
- [7] P. Hariharan, M. Roy, A geometric-phase interferometer, J. Modern Opt. 39 (1992) 1811–1815.
- [8] R. Simon, H.J. Kimble, E.C.G. Sudarshan, Evolving geometric phase and its dynamical manifestation as a frequency shift: An optical experiment, Phys. Rev. Lett. 61 (1988) 19–22.
- [9] T. Chyba, L.J. Wang, L. Mandel, R. Simon, Measurement of the Pancharatnam phase for a light beam, Opt. Lett. 13 (1988) 562–564.
- [10] S.P. Tewari, V.S. Ashoka, M.S. Ramana, A four-arm Sagnac interferometric switch, Opt. Commun. 120 (1995) 235–238.
- [11] B. Hils, W. Dultz, W. Martienssen, Nonlinearity of Pancharatnam's geometric phase in polarizing interferometers, Phys. Rev. E 60 (1999) 2322–2329.
- [12] E. Sjöqvist, Geometric phase for entangled spin pairs, Phys. Rev. A 62 (2000) 022109.
- [13] H. Kobayashi, Y. Ikeda, S. Tamate, T. Nakanishi, M. Kitano, Nonlinear behavior of geometric phases induced by photon pairs, Phys. Rev. A 83 (2011) 063808.
- [14] B. Décamps, A. Gauguet, J. Vigué, M. Büchner, Pancharatnam phase: A tool for atom optics, Phys. Rev. A 96 (2017) 013624.
- [15] R. Bhandari, Polarization of light and topological phases, Phys. Rep. 281 (1997) 1–64.
- [16] E. Galvez, Applications of geometric phase in optics, in: Recent Research Developments in Optics, Vol. 2, Research Signpost, Kerala, 2002, pp. 165–182.
- [17] S. Huard, Polarization of Light, John Wiley & Sons, New York, NY, 1996, Chapter 2.
- [18] J. Vickers, M. Burch, R. Vyas, S. Singh, Phase and interference properties of optical vortex beams, J. Opt. Soc. Amer. A 25 (2008) 823–827.